IEICE TRANS. COMMUN., VOL.E102–B, NO.3 MARCH 2019

PAPER

Bandwidth-Efficient Blind Nonlinear Compensation of RF Receiver Employing Folded-Spectrum Sub-Nyquist Sampling Technique

Kan KIMURA[†a)], ***Member and*** **Yasushi YAMAO**[†b)], ***Fellow***

SUMMARY Blind nonlinear compensation for RF receivers is an important research topic in 5G mobile communication, in which higher level modulation schemes are employed more often to achieve high capacity and ultra-broadband services. Since nonlinear compensation circuits must handle intermodulation bandwidths that are more than three times the signal bandwidth, reducing the sampling frequency is essential for saving power consumption. This paper proposes a novel blind nonlinear compensation technique that employs sub-Nyquist sampling analog-to-digital conversion. Although outband distortion spectrum is folded in the proposed sub-Nyquist sampling technique, determination of compensator coefficients is still possible by using the distortion power. Proposed technique achieves almost same compensation performance in EVM as the conventional compensation scheme, while reducing sampling speed of analog to digital convertor (ADC) to less than half the normal sampling frequency. The proposed technique can be applied in concurrent dual-band communication systems and adapt to flat Rayleigh fading environments.

key words: *blind nonlinear compensation, sub-nyquist sampling, spectrum-folding, fading, signal processing*

1. Introduction

Recently, mobile communication traffic is increasing remarkably with the spread of smart phones and various applications. In order to achieve higher data rate and increase system capacity, enhanced radio spectrum utilization techniques including inter-band career aggregation and multiple access over heterogeneous multiband networks [1] are considered in the 5G system [2]. In such concurrent multiband and multi-access operation, the received signal envelope of respective signals fades independently among different RF bands. Thus, the resultant multiband received signal presents large variation of signal envelope, which increases the chance to generate nonlinear distortions in a receiver front-end due to inter-modulation and cross-modulation [3]. Then the received signals suffer from the nonlinear distortions and the error vector magnitude (EVM) values deteriorate. It limits the chance to use higher level modulation such as 256 QAM and system performance will be degraded.

Blind nonlinear compensation techniques for RF receiver have been proposed as an effective countermeasure for the issue [3]–[7]. They realize post-compensation functions by baseband digital signal processing as well as other necessary decoding process in the receiver. Therefore the techniques can improve the linearity of the receiver without adding any RF circuits. However, the techniques increase power consumption of the receiver because nonlinear distortion has 3 to 5 times wider bandwidth of the original signals, which results in higher sampling/processing frequency compared with linear processing. Higher speed analog to digital convertors (ADCs) consume much power and are expensive. Therefore, reduction of sampling frequency is important for the blind nonlinear compensation techniques.

In the area of nonlinear transmitter compensation, several sampling frequency reduction techniques have been proposed for digital predistorters (DPDs) [8]–[12], In Ref. [8], subsampling, or bandpass sampling, was applied in the feedback loop of concurrent dual-band DPD for reducing the complexity and power consumption of multiple down converters. Reference [9] limits the feedback bandwidth before narrowband ADC and recovers the lost part of band-limited spectrum by an extrapolation technique. Reference [10] allows the use of an under-sampling ADC in the DPD feedback path to sample wideband PA output signals and restore the full-band PA output information. However, none of the above techniques can compensate receiver nonlinearity because they need the original signal as the reference, which is not available in the receiver.

This paper proposes a novel blind nonlinear compensation method that employs folded-spectrum sub-Nyquist sampling ADC. In the method, received signal is sampled by a low-speed ADC without prior bandwidth limitation process such as anti-aliasing filtering. As a result, the received signal samples are sparse and it's outband distortion spectrum is folded. However, the samples still keep sufficient amplitude information of the original signal, and nonlinear compensation is possible by utilizing the folded outband distortion power. Consequently, the proposed technique can reduce sampling speed of ADC to less than half the normal sampling frequency, while maintaining almost same compensation performance as that of conventional schemes.

The organization of this paper is as follows: Sect. 2 begins with the principle of the proposed blind nonlinear compensation with sub-Nyquist sampling. Section 3 discusses the signal processing parameter design for the proposed scheme based on the simulation results. Performance of the proposed nonlinear compensator is evaluated in terms of error vector magnitude (EVM) and convergence time. In Sect. 4, the proposed architecture is extended to concurrent dual-band operation. Measured performance by ex-

Manuscript received April 3, 2018.
Manuscript revised August 4, 2018.
Manuscript publicized September 14, 2018.

[†]The authors are with the Advanced Wireless Communication & Research Center, The University of Electro-Communications, Chofu-shi, 182-8585 Japan.
a) E-mail: k.kimura@awcc.uec.ac.jp
b) E-mail: yyamao@m.ieice.org

DOI: 10.1587/transcom.2018EBP3100

periments is presented in Sect. 5 to validate the simulation, which is followed by a conclusion in Sect. 6.

2. Principle

2.1 Blind Nonlinear Compensation

Figure 1 shows the diagram of proposed blind nonlinear compensation scheme. Received signals are affected by the nonlinearity of RF front-end including low noise amplifier (LNA) and down conversion mixer. Distorted signals are down-converted to baseband and digitized by an ADC after passing through an anti-aliasing filter with a cut-off frequency of BW_{aa}. A blind nonlinear compensator suppresses the nonlinearity by using the nonlinear model that is memoryless power series in baseband and given by

$$z(t) = \sum_{k=1}^{D} b_k \, |y(t)|^{k-1} \, y(t) \tag{1}$$

Here, D is the maximum order of nonlinearity and b_k is the coefficient of nonlinear compensator.

In the blind nonlinear compensator for RF receiver, the compensation system has no previous knowledge on the original signal except for its bandwidth. Considering that nonlinear distortion spectra always appear in the sidebands of signal due to intermodulation (IM) process, out-of-band radiation power can be employed as the cost function. Coefficient vector $\boldsymbol{b}$ is determined to minimize the cost function [4]. For this purpose, it is necessary to collect the sufficient number of receiver output samples and calculate the outband radiated distortion. Hereafter we consider time series sample vectors for y(t) and $z(t)$, such as $\boldsymbol{y} = (y_1, y_2, \cdots y_N)$ and $\boldsymbol{z} = (z_1, z_2, \cdots z_N)$.

After compensation has completed, compensator output $\boldsymbol{z}$ and outband noise rejection LPF output $\boldsymbol{u}$ can be equal to the original signal. Therefore, coefficient vector $\boldsymbol{b}$ can be determined using Least Square method (LS) [5]. Equation used for coefficient determination is given by

$$\boldsymbol{b} = \left(\mathbf{Y}^{\mathbf{H}}\mathbf{Y}\right)^{-1} \mathbf{Y}^{\boldsymbol{H}} \boldsymbol{u}, \tag{2}$$

$$\mathbf{Y} = \begin{bmatrix} \boldsymbol{y} \\ |\boldsymbol{y}|\,\boldsymbol{y} \\ \vdots \\ |\boldsymbol{y}|^{\boldsymbol{D-1}}\,\boldsymbol{y} \end{bmatrix}^{\mathbf{T}}, \tag{3}$$

$$\boldsymbol{b} = [b_1 b_2 \cdots b_D]^{\mathrm{T}}, \tag{4}$$

$$\boldsymbol{u} = \boldsymbol{h} * \boldsymbol{z}, \tag{5}$$

where $\boldsymbol{h}$ is the impulse response of outband rejection LPF, $*$ is the convolution operator.

2.2 Sampling Method in Nonlinear Compensation

From the sampling theorem, the original signal can be perfectly reproducted from the sampled signal if sampling frequency is set more than twice of the original signal bandwidth. Since nonlinear distortion has 3 to 5 times wider

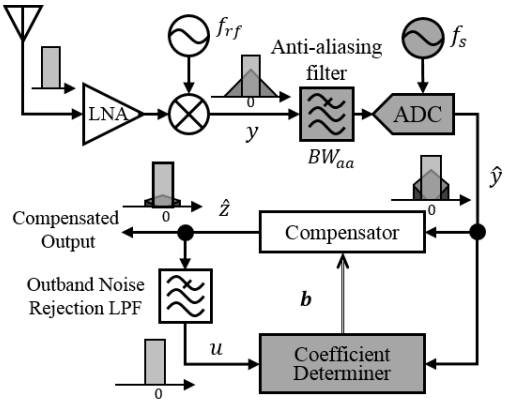

Fig. 1 Proposed blind nonlinear compensation scheme with sub-Nyquist sampling technique.

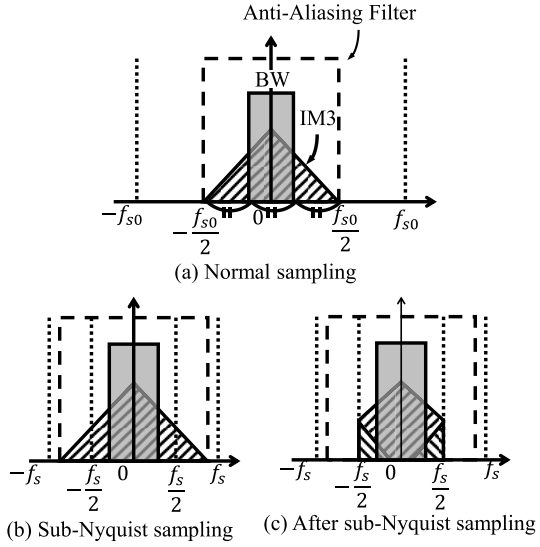

Fig. 2 Normal and proposed sampling methods in A/D conversion.

bandwidth than that of the original signal, it is natural to think that ADC in the blind nonlinear compensator needs 3 to 5 times higher sampling frequency compared with that for linear signal sampling. The spectra of normal sampling and proposed folded-spectrum sub-Nyquist sampling (FS-SNS) are illustrated in Fig. 2. In Fig. 2(a), the sampling frequency f_{s_0} of normal sampling is set more than twice of the input signal bandwidth including nonlinear distortion. The cutoff frequency of anti-aliasing filter (AAF) before ADC is set $f_{s_0}/2$ or higher to avoid aliasing. In general, the most dominant and harmful nonlinear distortion component is the third-order intermodulation (IM3) and its bandwidth is three times of the original signal bandwidth. Then the normal sampling frequency f_{s_0} should be six times higher than the original signal bandwidth to satisfy the sampling theorem.

In Fig. 2(b), sampling frequency f_s is set less than twice of the input signal bandwidth but more than twice of the original signal bandwidth, whereas the cutoff frequency of AAF is same as that of normal sampling to pass all input signal band including nonlinear distortion. In this method,

some part of outband distortion is folded back under Nyquist frequency (Fig. 2(c)). Comparing Fig. 2(a) and Fig. 2(c), it is found that the original signal is maintained because the sub-Nyquist sampling frequency is high enough to reproduct the original signal. Although some part of the nonlinear distortion is folded, its power is maintained in total. Since the goal of the nonlinear compensation scheme is to minimize the distortion power, it is expected that the spectrum folding of outband distortion will not cause any serious problem.

2.3 Blind Nonlinear Compensation Employing FS-SNS

In order to validate the proposal, discrete-time signal processing in nonlinear compensation should be discussed before going into the detailed design.

If the AAF can pass all input signal including nonlinear distortion, the sampled signal $\hat{y}$ in continuous-time expression is given by

$$\hat{y}(t) = y(t)s(t), \tag{6}$$

$$s(t) = \sum_{n=-\infty}^{\infty} \delta(t - n\mathrm{T}), \tag{7}$$

where $s(t)$ is the sampling function, $\delta(t)$ is the delta function, T is sampling interval, and n is sample number. By substituting Eq. (6) to Eq. (1), sampled compensator output $\hat{z}$ in continuous-time expression is given by

$$\begin{aligned}\hat{z}(t) &= \sum_{k=1}^{D} b_k \left|\hat{y}(t)\right|^{k-1} \hat{y}(t) \\ &= \sum_{k=1}^{D} b_k \left|y(t)s(t)\right|^{k-1} y(t)s(t) \\ &= \sum_{k=1}^{D} b_k \left|y(t)\right|^{k-1} y(t) \left|s(t)\right|^{k-1} s(t).\end{aligned} \tag{8}$$

Since $s(t)$ is a non-negative real function and multiple sampling operation is identical to single sampling operation,

$$|s(t)|^{k-1}\, s(t) = s^k(t) = s(t), \tag{9}$$

$$\hat{z}(t) = s(t) \sum_{k=1}^{D} b_k |y(t)|^{k-1} y(t). \tag{10}$$

Equation (10) represents the sampled signal of the nonlinear-compensated continuous-time signal. Therefore, nonlinear compensation after sampling and sampling after nonlinear compensation are equivalent. Consequently, sampled nonlinear signal with any sampling frequency can be compensated if it can be compensated in the continuous-time domain.

On the other hand, there is restriction that sampling frequency f_s of the proposed FS-SNS method should be higher than the original RF signal bandwidth BW, as shown in Fig. 2. Since the normal sampling frequency f_{s_0} is set more than the nonlinear input signal bandwidth 3BW, it is necessary that

$$\frac{f_s}{f_{s_0}} > \frac{1}{3}. \tag{11}$$

Above condition shows a lower limit of f_s. Actual limit of f_s in the proposed scheme is determined by the convergence time of the compensator. If the sampling frequency is low, a longer time is necessary to collect a necessary number of samples. The necessary number of samples to achieve good performance will be discussed in the later section.

2.4 Nonlinear Compensation for Dual-Band Operation

Recently, concurrent multiband access is commonly employed to increase the system throughput. In the LTE system, it is called inter-band carrier aggregation (CA). If the separation of two RF bands is not so wide, the antenna and LNA are shared between two bands. The configuration of proposed blind nonlinear compensation scheme for dual-band operation is shown in Fig. 3. In the figure, local frequencies f_{rf1} and f_{rf2} are the center frequencies of two bands. Signals of the two bands are down-converted to baseband separately after distorted by the front-end. Baseband signals are A/D converted with FS-SNS and their distortions are compensated by two blind nonlinear compensators with coefficient vectors of $\boldsymbol{c}^{(1)}$ and $\boldsymbol{c}^{(2)}$

The most important difference from Fig. 1 in the signal processing of blind nonlinear compensation is that the compensation should consider two independently fluctuated input signals in each compensator [3]. Therefore, nonlinear model of Eq. (1) should be modified to the following dual-band nonlinear baseband model.

$$z^{(1)} = \sum_{k=0}^{(D-1)/2} \sum_{l=0}^{k} c^{(1)}_{2(k-l),2l} \left|y^{(1)}\right|^{2(k-l)} \left|y^{(2)}\right|^{2l} y^{(1)}, \tag{12}$$

$$z^{(2)} = \sum_{k=0}^{(D-1)/2} \sum_{l=0}^{k} c^{(2)}_{2(k-l),2l} \left|y^{(1)}\right|^{2(k-l)} \left|y^{(2)}\right|^{2l} y^{(2)}. \tag{13}$$

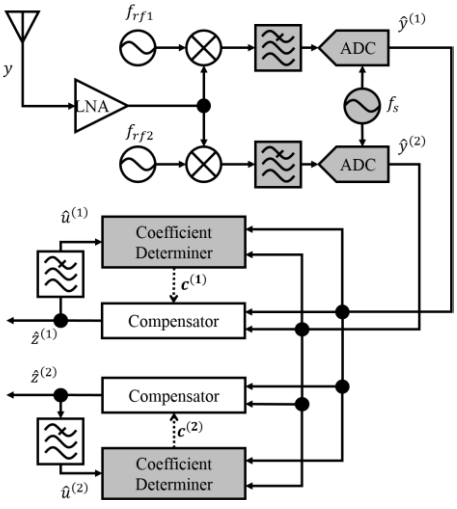

Fig. 3 Proposed blind nonlinear compensation scheme for dual-band operation.

Here, $y^{(1)}$ and $y^{(2)}$ represent distorted signals for the center frequencies of f_{rf1} and f_{rf2}, respectively. $c^{(1)}_{2(k-l),2l}$ and $c^{(2)}_{2(k-l),2l}$ are the coefficient sets of two nonlinear compensators. In the vicinity of signal bands, odd-order nonlinear components are dominant and even-order components can be ignored [4]. Then, coefficient vector $\boldsymbol{c}^{(1)}$ for the band centered at f_{rf1} is given by

$$\boldsymbol{c}^{(1)} = \left(\boldsymbol{Y}^{(1)\mathrm{H}}\boldsymbol{Y}^{(1)}\right)^{-1}\boldsymbol{Y}^{(1)\mathrm{H}}\boldsymbol{u}^{(1)}, \tag{14}$$

$$\boldsymbol{Y}^{(1)} = \begin{bmatrix} \boldsymbol{y}^{(1)} \\ \left|\boldsymbol{y}^{(1)}\right|^2 \boldsymbol{y}^{(1)} \\ \left|\boldsymbol{y}^{(2)}\right|^2 \boldsymbol{y}^{(1)} \\ \vdots \\ \left|\boldsymbol{y}^{(2)}\right|^{D-1} \boldsymbol{y}^{(1)} \end{bmatrix}^{T}, \tag{15}$$

$$\boldsymbol{c}^{(1)} = \begin{bmatrix} c_{0,0} & c_{2,0} & c_{0,2} & \cdots & c_{0.D-1} \end{bmatrix}^{\mathrm{T}}, \tag{16}$$

$$\boldsymbol{u}^{(1)} = \boldsymbol{h}^{(1)} * \boldsymbol{z}^{(1)}. \tag{17}$$

Here, $\boldsymbol{h}^{(1)}$ is the impulse response of outband rejection LPF for signal 1. The other compensator coefficient vector $\boldsymbol{c}^{(2)}$ is estimated similarly.

3. Performance Evaluation by Simulations

In this section, the relationship between design parameters and compensation performance is analyzed through computer simulations with MATLAB. Compensation performance is evaluated in terms of attainable Error Vector Magnitude (EVM) and convergence time to clear 3% EVM.

3.1 Nonlinear Model of RF Frontend

Saleh model [13] is commonly used for representing the nonlinearity of RF amplifiers. It is employed in the simulation as the nonlinear model of RF frontend circuit. Nonlinear characteristic of this model is given by

$$\mathrm{AM/AM} = \frac{\alpha_A r}{1+\beta_A r^2}, \tag{18}$$

$$\mathrm{AM/PM} = \frac{\alpha_P r^2}{1+\beta_P r^2}. \tag{19}$$

Here r is the amplitude of input signal. $\alpha_{A,p}$ and $\beta_{A,p}$ are the parameters that determine nonlinear characteristic. In the simulation, $\alpha_A, \beta_A, \alpha_P$ and β_P are set 2, 1, $-(\pi/3)$ and 1, respectively, as typical values. The nonlinear output spectrum of the LTE signal/10 MHz RF channel by using this model with 10 dB back-off is shown in Fig. 4. The bandwidth for distortion level of −40 dB down from the signal level is 28 MHz, which is around three times wider than the original signal. It indicates that the dominant distortion component generated by the model is the third intermodulation (IM3).

3.2 Basic Settings for Simulation

Table 1 summarizes basic simulation settings. LTE signal for 10 MHz RF channel is used as the test signal. Signal input level is back-offed by 10 dB to obtain the EVM of around 12%, where third order distortion (IM3) is dominant. We choose the maximum order of five for the power series of compensator to obtain the inverse characteristic of nonlinearity [14]. An ideal rectangular filter by fast Fourier Transform (FFT) is employed as the outband noise rejection LPF in Fig. 1. The FFT size is determined by the signal processing block size described in the next section.

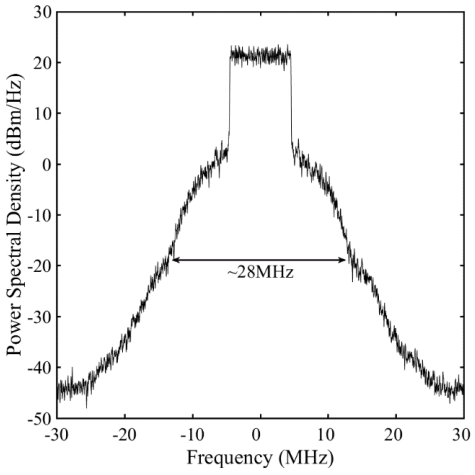

Fig. 4 Nonlinear output spectrum of LTE signal based on Saleh model.

Table 1 Basic Simulation Settings.

Signal	LTE / 64QAM
Occupied RF bandwidth	9.03 MHZ
Sampling frequency (f_s)	11, 12, 14, 18, 30 MHz
Signal processing block size (bs)	128 – 4096 samples
LNA back-off	10 dB
SNR	60 dB
Max. order of compensation	5
Anti-aliasing filter cut-off freq.	15 MHz

3.2.1 Signal Processing Block Size

As mentioned in Sect. 2.1, sufficient number of receiver output samples should be collected to calculate the outband radiated distortion and determine coefficient vector $\boldsymbol{b}$. If the number is not enough, calculated $\boldsymbol{b}$ fluctuates due to residual error and compensation performance is degraded. Hereafter we refer the number of samples as "*signal processing block size*" denoted by b_S.

On the other hand, smaller block size is preferred to implement compensator circuit compact. Figure 5 shows relationship between signal processing block size and achieved EVM at various sampling frequencies including 30 MHz as normal sampling and 11 to 18 MHz as sub-Nyquist sampling frequencies. From the figure, the block size of 1024 samples is enough for any sampling frequency. If the block size is less than 1024 samples, attainable EVMs increase and present differences among sampling frequencies. Since

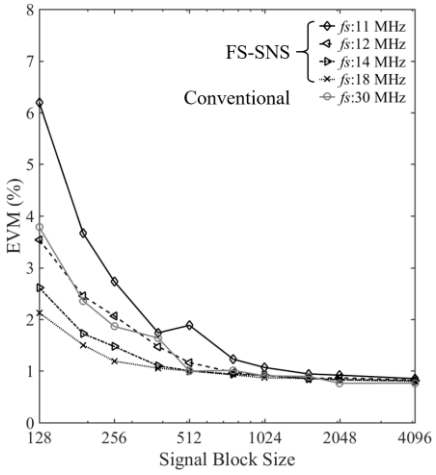

Fig. 5 Simulated EVM vs. signal processing block size.

FFT size for signal outband rejection LPF is determined by the signal processing block size, small block size affects resolution in frequency domain and causes deterioration of outband rejection LPF characteristic.

3.2.2 Convergence Time

Convergence time is an important performance of the receiver nonlinear compensation because the input signal power always changes and sometimes fades out temporally. Considering the previous results, signal processing block size bs is determined as 1024 samples. Convergence times is calculated as $S_N \times b_S / f_s$. Here, S_N is the number of steps required for convergence. Figure 6 shows the EVM convergence characteristic for different sampling frequencies. It is obvious from the figure that convergence time depends on the sampling frequency. Since convergence time is determined as the product of signal block duration and the number of its iteration, it is basically inverse-proportional to the sampling frequency. When sampling frequency is 14 MHz, which is less than half of the normal sampling frequency of 30 MHz, convergence time is less than 0.4 ms. FS-SNS with less than 14 MHz sampling frequency needs extra convergence time than that calculated from the inverse-proportional relation to the sampling frequency.

3.3 Performance in Rayleigh Fading Environment

From the convergence performance in the previous section, it is expected that the proposed system can operate under fast fading environments. The convergence time of 0.4 ms is enough for covering the maximum Doppler frequency of 100 Hz. Therefore, compensation performance in fast Rayleigh fading environment is studied by using computer simulations. Signal processing block size and sampling frequency are set 1024 samples and 14 MHz, respectively. The other parameters are same as in Table 1. The same LTE signal for RF bandwidth of 10 MHz is used as a test signal.

After the LTE signal sample stream is generated in complex baseband according to the specification, it is multiplied by the Rayleigh fading complex weight stream that has the maximum Doppler frequency of either 30 Hz or 100 Hz. The faded signal is fed to the RF front end of the proposed post-compensation receiver. The fading weight stream is generated from the random sequence and its length is set far longer than the signal stream length. The seed parameters for creating the streams are randomly changed at each time of the creation, and simulated results are averaged.

Figure 7 shows simulation results for the maximum Doppler frequency (f_D) of 30 Hz. The normalized envelops for a faded input signal and its distorted signal are shown in Fig. 7(a). Time variation of EVM is shown in Fig. 7(b) with the same time line as Fig. 7(a). From the figures, it is

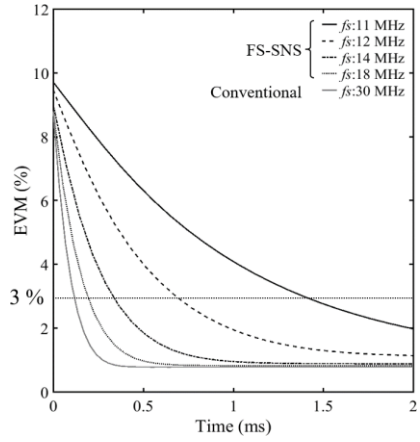

Fig. 6 Simulated EVM convergence v.s. sampling frequency.

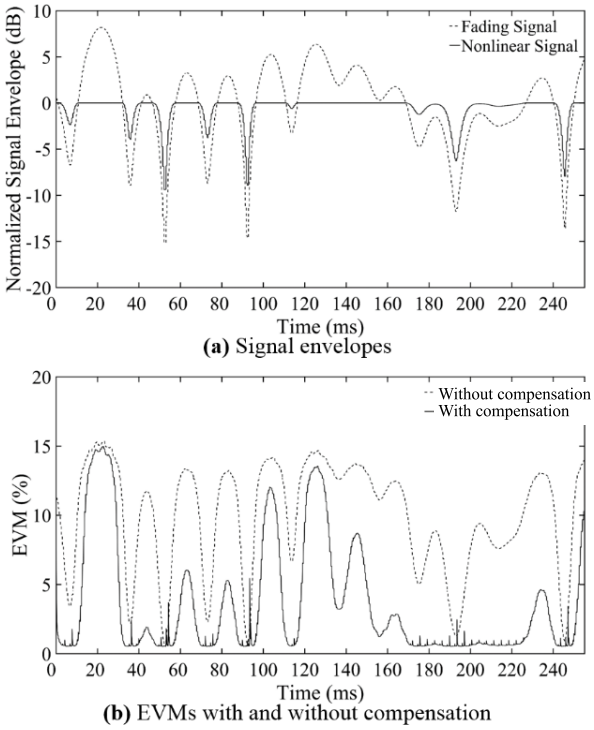

Fig. 7 Simulated EVM for Rayleigh faded channel (f_D: 30 Hz).

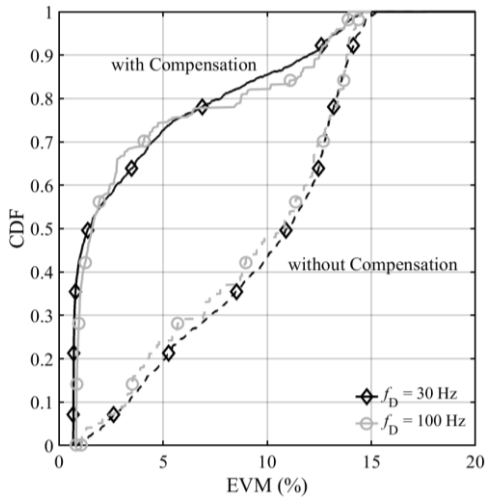

Fig. 8 CDF of EVM for Rayleigh Faded Channel (f_D = 30, 100 Hz).

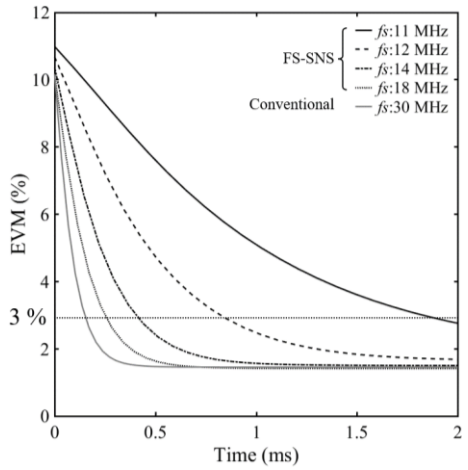

Fig. 9 Simulated EVM convergence of Sig1 vs. sampling frequency for dual-band operation.

confirmed that EVM with the compensator accurately traces fading fluctuation and is improved most of time. When the signal envelope is smaller than −15 dB, compensator output sometimes presents discontinuous large EVM. This is due to the decrease of the input signal power. However, nonlinear compensation is not necessary for such low input power level. Since the compensator can converged quickly just after the input power has recovered, this problem can be solved by switching compensation mode and linear mode according to the input power by monitoring RSSI.

Figure 8 shows the CDF of EVM for Rayleigh faded channel in the same condition as Fig. 7. The results for two maximum Doppler frequency cases are presented. The CDFs for both cases are similar, which suggests that the proposed compensation method can successfully traces the fading fluctuation for the f_D of 100 Hz or less. From the figure, the time probability of exceeding EVM of 5% for the f_D of 100 Hz is reduced to 25% from 75% of non-compensated output. Therefore, the proposed compensator can improve the EVM in the time ratio of 50% in average. The improvement of EVM contributes much to increase the chance of using higher-level modulation schemes such as 64 QAM and 256 QAM. Therefore, system throughput can be increased.

3.4 Performance of Dual-Band Compensation

We assume two frequency band signals, Sig1 and Sig2, with center frequencies of 2.0 GHz and 2.4 GHz, respectively, for performance evaluation of the proposed dual-band compensator by simulation. Influences of different power levels and signal bandwidth are also examined.

3.4.1 Convergence Time of Dual-Band Operation

Figure 9 shows EVM convergence characteristic for the dual-band compensator. Both signal bandwidth are set to 10 MHz, same as the single band compensator. Convergence characteristics of two signals are similar as that of the single band. However, the achievable EVM and convergence time of the dual-band compensator increase slightly compared with those of the single band. Nevertheless, they can still keep less than 2% and 0.5 ms for the same sampling frequency of 14 MHz.

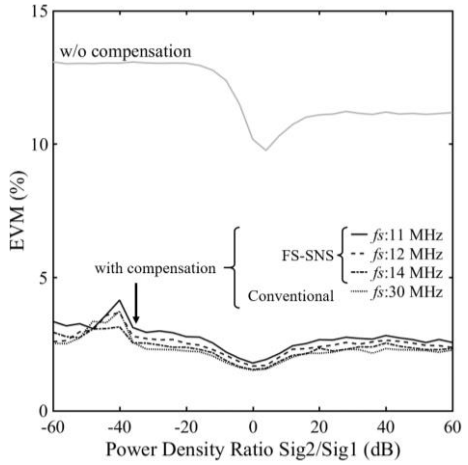

Fig. 10 EVM of Sig2 vs. power density ratio (equal bandwidth).

3.4.2 Influence by Different Power Density

In concurrent multiband access systems, the signals are faded independently. Moreover, multiple access over heterogeneous multiband networks is considered in 5G, where the signals are transmitted from different places such as macro- and femto- base stations. Then, the deviation of two received signal power can be quite large.

Figure 10 shows relationship between signal power density ratio and achievable EVM. Both signal bandwidths are set to 10 MHz. Signal power spectral density ratio of two signals, Sig2 to Sig1, is varied from −60 dB to 60 dB. From the figure, EVM without compensation is more than 10% for both signals. When power density ratio is one (0 dB), compensator provides the best performance in both

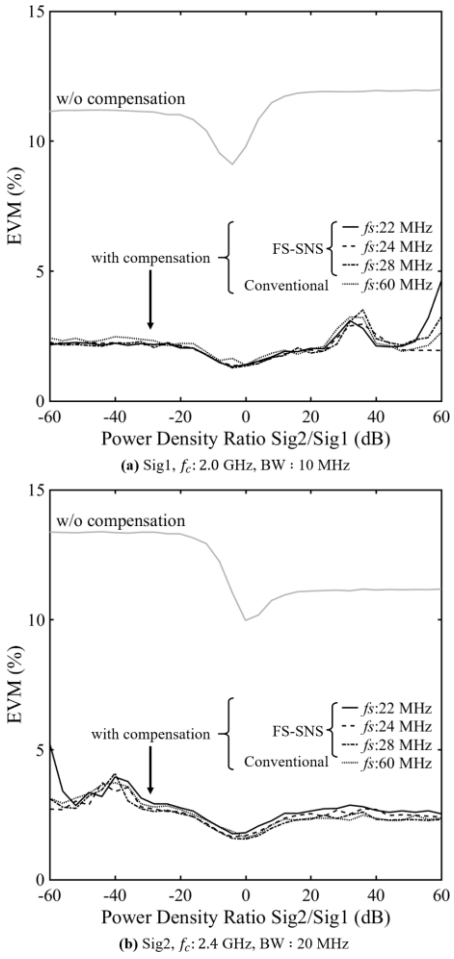

Fig. 11 EVM vs. power density ratio for unequal signal bandwidth.

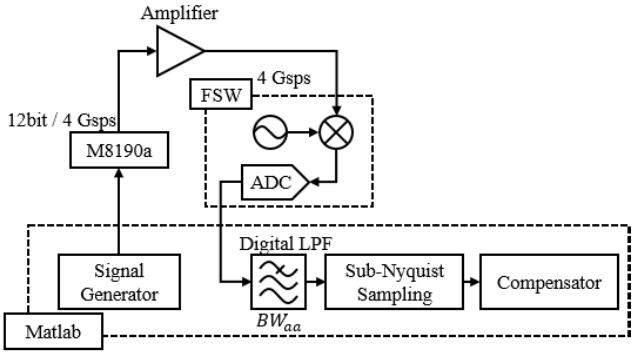

Fig. 12 Block diagram of experimental setup.

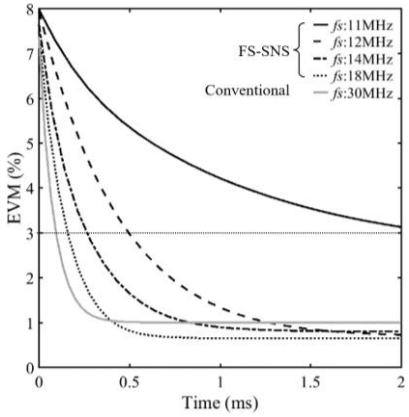

Fig. 13 Measured EVM convergence vs. sampling frequency.

bands and EVM is less than 2%. Although much smaller or larger power density ratios deteriorate the compensator performance, EVM still keeps less than 3% for f_s of 14 MHz.

3.4.3 Influence by Different Signal Bandwidth

When a concurrent multiband system transmits signals with different bandwidths, the sampling frequency of dual-band compensator should cover the wider bandwidth.

Assuming a dual-band signal that bandwidths are 10 MHz for SIG1 and 20 MHz for SIG2, sampling frequency is doubled and varied from 22 MHz to 60 MHz for capturing the 20 MHz-bandwidth signal. Power density ratio is varied from −60 dB to 60 dB. Figure 11 shows relationship between signal power density ratio and EVM on different signal bandwidth. From the figure, nonlinear compensation characteristic is similar to that for equal bandwidth case.

4. Performance Evaluation by Experiment

In order to confirm the basic performance of the proposed FS-SNS nonlinear compensation, experiments were conducted. Default signal processing block size and sampling frequency are set 1024 samples and 14 MHz, respectively.

4.1 Experimental Setup

Experimental setup is shown in Fig. 12. The MATLAB program generates LTE signal data stream of 10 MHz channel in baseband. Then Arbitrary Signal Generator M8190A by Keysight Technologies generates the RF signal with a carrier frequency of 920 MHz. After amplified by a small output power amplifier of R & K A100H-G and AA160, the signal analyzer FSW by Rohde & Schwarz captures and buffered the distorted signal as a high-speed ADC. Buffered stream data is sent to the SF-SNS compensator MATLAB program and EVM and ACLR are calculated.

4.2 Experimental Results

Figure 13 shows EVM convergence curves for different sampling frequencies. The curves show the same tendency as the simulated results in Fig. 6, except for the 11 MHz sampling frequency case. Obtained convergence times are summarized in Table 2 with the simulated values. Except for the case of 11 MHz, convergence times are shorter than the simulated results. This is considered to happen due to the difference of nonlinear characteristic between simulation model and actual amplifier. From the experimental results,

Table 2 Convergence time for 3% EVM.

Sampling Frequency (MHz)	30	18	14	12	11
Simulation (ms)	0.17	0.28	0.43	0.85	2.0
Experiment (ms)	0.1	0.17	0.28	0.5	2.27

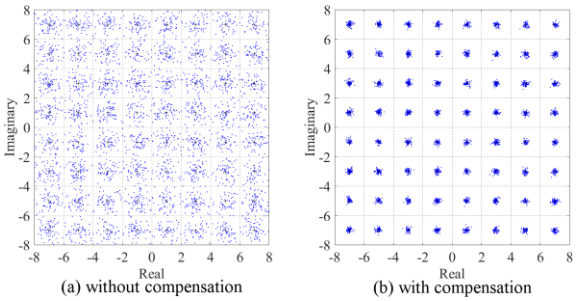

Fig. 14 64QAM constellations with and without compensation.

it is confirmed that the proposed scheme with sampling frequency of 12 MHz or higher achieves fast convergence time of 0.5 ms.

Figure 14 shows LTE 64 QAM constellations with and without compensation. From the constellation diagrams, it is clear that the proposed blind nonlinear compensator improves the EVM quite successfully.

5. Conclusion

This paper proposed a novel blind nonlinear compensation method using folded-spectrum sub-Nyquist sampling ADC. We analyzed the relationship between processing parameters and compensation performance in terms of EVM and convergence time. Necessary sampling frequency for compensating IM3 distortion is reduced to around three times of the IQ bandwidth, which is less than half of the normal Nyquist sampling. Compensator coefficients can be converged in less than 0.5 ms, which enables the proposed method to work under fast Rayleigh fading environment. The proposed scheme can reduce necessary ADC sampling frequency and save energy. It will improve receiver performance in future broadband wireless systems and contribute to enhance system performances. Implementation of the compensator in real receivers remains as the future work.

References

[1] S.A. Bassam, W. Chen, M. Helaoui, and F.M. Ghannouchi, "Transmitter architecture for CA: Carrier aggregation in LTE-advanced systems," IEEE Microw. Mag., vol.14, no.5, pp.78–86, 2013.
[2] T. Specification, G. Radio, A. Network, N. Generation, and A. Technologies, "3GPP TR 38.913," vol.0, no.Release 14, 2017.
[3] Y. Ma, Y. Yamao, K. Ishibashi, and Y. Akaiwa, "Adaptive compensation of inter-band modulation distortion for tunable concurrent dual-band receivers," IEEE Trans. Microw. Theory Techn., vol.61, no.12, pp.4209–4219, 2013.
[4] M. Valkama, H. Shahed, L. Anttila, and M. Renfors, "Advanced digital signal processing techniques for compensation of nonlinear distortion in wideband multicarrier radio receivers," IEEE Trans. Microw. Theory Techn., vol.54, no.6, pp.2356–2366, June 2006.
[5] G. Hueber, Y. Zou, K. Dufrene, R. Stuhlberger, and M. Valkama, "Smart front-end signal processing for advanced wireless receivers," IEEE J. Sel. Topics Signal Process., vol.3, no.3, pp.472–487, June 2009.
[6] Y. Ma and Y. Yamao, "Blind nonlinear compensation technique for RF receiver front-end," Proc. 43rd Eur. Microw. Conf., pp.1527–1530, 2013.
[7] Y. Liu, "Adaptive blind postdistortion and equalization of system impairments for a single-channel concurrent dual-band receiver," IEEE Trans. Microw. Theory Techn., vol.65, no.1, pp.302–314, 2017.
[8] S.A. Bassam, A. Kwan, W. Chen, M. Helaoui, and F.M. Ghannouchi, "Subsampling feedback loop applicable to concurrent dual-band linearization architecture," IEEE Trans. Microw. Theory Techn., vol.60, no.6, pp.1990–1999, May 2012.
[9] Y. Ma, Y. Yamao, Y. Akaiwa, and K. Ishibashi, "Wideband digital predistortion using spectral extrapolation of band-limited feedback signal," IEEE Trans. Circuits Syst. I, Reg. Papers, vol.61, no.7, pp.2088–2097, 2014.
[10] Y. Liu, J.J. Yan, H. Dabag, S. Member, and P.M. Asbeck, "Novel technique for wideband digital predistortion of power amplifiers with an under-sampling ADC," IEEE Trans. Microw. Theory Techn., vol.62, no.11, pp.2604–2617, 2014.
[11] Q. Zhang, W. Chen, Z. Wang, and G. Su, "A single feedback architecture for dual-band digital predistortion with under-sampling technique," Proc. IEEE MTT-S 2016, Shanghai, 2016.
[12] A.K. Jain and S. Ranganath, "Extrapolation algorithms for discrete signals with application in spectral estimation," IEEE Trans. Acoust., Speech, Signal Process., vol.29, no.4, pp.830–845, 1981.
[13] A.A.M. Saleh, "Frequency-independent and frequency-dependent nonlinear models of TWT amplifiers," IEEE Trans. Commun., vol.29, no.11, pp.1715–1720, 1981.
[14] Y. Ma, Y. Akaiwa, and Y. Yamao, "Fast baseband polynomial inverse algorithm for nonlinear system compensation," IEEE Veh. Technol. Conf., pp.1–5, 2012.

Kan Kimura received the B.S. and M.S. degrees in Electrical Engineering from the University of Electro-Communications in 2016 and 2018, respectively. His research interest is in nonlinear compensation using digital signal processing technologies.

Yasushi Yamao received his B.S., M.S., and Ph.D. degrees in electronics engineering from Kyoto University, Kyoto, Japan, in 1977, 1979, and 1998, respectively. He started his research career of mobile communications from the measurement and analysis of urban radio propagation as his M.S. thesis. In 1979, he joined the Nippon Telegraph and Telephone Corporation (NTT) Laboratories, Japan, where his major activities included leading research on GMSK modulator/demodulator and GaAs RF ICs for digital mobile communications, and development of PDC digital cellular handheld phones. In 1993, he moved to NTT DoCoMo Inc. and directed standardization of high-speed paging system (FLEX-TD) and development of 3G radio network system. He also joined European IST research programs for IP-based 4th generation mobile communication. In 2005, he moved to the University of Electro-Communications as a professor of the Advanced Wireless Communication Research Center (AWCC). Now he is the director of AWCC. His current interests focus on wireless ubiquitous communication networks and protocols, as well as high-efficiency and reconfigurable wireless circuit technologies both in RF and Digital Signal Processing. Prof. Yamao is a Fellow of the IEICE and member of the IEEE and IPSJ. He served as the Vice President of IEICE Communications Society (2003–2004), the Chairman of IEICE Technical Group on Radio Communication Systems (2006–2008), the Chief Editor of IEICE Communication Magazine (2008–2010), the Vice chairman of IEEE VTS Japan chapter (2009–2015), and a Director of the IEICE (2015–2017).